Hybrid IRS–NOMA Framework for Turbulence Resilient Underwater Visible Light Communication

Prathibha Praharsha Sripathi, *Student Member, IEEE*, and Mahesh Miriyala, *Member, IEEE*

***Abstract*—Underwater Visible Light Communication (UVLC) offers high data rates, low latency, and strong physical-layer security, making it as an alternative to acoustic and RF systems for real-time underwater applications. However, its performance is severely degraded by absorption, scattering, and turbulence-induced fading. To enhance link reliability, recent advances in Non-Orthogonal Multiple Access (NOMA) and Intelligent Reflecting Surfaces (IRS) are being integrated into UVLC systems. NOMA enables simultaneous multi-user access through power-domain multiplexing, improving spectral efficiency and connectivity, while IRS enhances signal strength and coverage by intelligently reflecting and directing optical beams. Motivated by these benefits, we propose a hybrid IRS–NOMA framework for UVLC to improve link reliability and mitigate turbulence effects. A composite channel model is formulated by combining direct and IRS-reflected paths under absorption, scattering, and turbulence modeled using the Exponential Generalized Gamma (EGG) distribution with pointing errors. Closed-form expressions for the outage probability and average bit error rate (ABER) are derived in terms of the Meijer-G function. System performance is evaluated under various configurations, and Monte Carlo simulations validate the analytical results, demonstrating excellent match and highlighting the effectiveness of the proposed IRS–NOMA-assisted UVLC design.**

Link to graphical and video abstracts, and to code:
https://latamt.ieeer9.org/index.php/transactions/article/view/10373

***Index Terms*—EGG Distribution, Intelligent Reflecting Surface (IRS), Non-Orthogonal Multiple Access (NOMA), Underwater Visible Light Communication (UVLC).**

I. Introduction

THE growing demand for high-speed, reliable, and secure underwater communication has generated significant interest in Underwater Visible Light Communication (UVLC) as an alternative to traditional acoustic and radio-frequency (RF) technologies [1]. RF signals experience rapid attenuation in seawater, limiting their effective transmission range. On the other hand, acoustic waves support long-distance communication but suffer from low data rates and substantial propagation delays. UVLC overcomes these limitations by offering wide bandwidth, low latency, and immunity to electromagnetic interference, making it well suited for a wide range of applications, including underwater sensor networks, autonomous underwater vehicles (AUVs), environmental monitoring, and defense operations [2].

The associate editor coordinating the review of this manuscript and approving it for publication was Carolina Del-Valle-Soto (*Corresponding author: Mahesh Miriyala*).

P. P. Sripathi and Mahesh Miriyala are with School of Electronics Engineering, VIT-AP Univeristy, Amaravati, India (e-mails: prathibha.23phd7191@vitap.ac.in, and mahesh.m@vitap.ac.in).

Despite these advantages, UVLC performance is heavily constrained by underwater channel impairments such as absorption, scattering, and particularly turbulence-induced fading, all of which cause random fluctuations in the received optical intensity and degrade link reliability [3]. To address these challenges, researchers have explored the integration of advanced communication and signal-processing techniques into UVLC systems. Among these, Non-Orthogonal Multiple Access (NOMA) and Intelligent Reflecting Surfaces (IRS) have recently emerged as promising solutions [4].

NOMA has emerged as a promising multiple-access technique for UVLC systems, offering enhanced spectral efficiency, reduced latency, and support for massive connectivity. Unlike conventional orthogonal access schemes, NOMA allows multiple users to simultaneously share the same time–frequency resources by exploiting the power domain, typically employing linear superposition coding (SC) at the transmitter and successive interference cancellation (SIC) at the receiver. By allocating higher transmit power to far users and lower power to near users, NOMA enhances both spectral efficiency and user fairness compared to Orthogonal Multiple Access (OMA) [5].

Several studies have investigated the application of NOMA in UVLC systems under diverse underwater channel conditions. The authors in [6] analyzed a NOMA-assisted UVLC system modeled with Exponential–Generalized Gamma (EGG) fading, deriving closed-form expressions for the average BER and ergodic capacity while examining the influence of bubble concentration, temperature gradients, and salinity. Their results indicate that system performance degrades as bubble levels and salinity increase, with bubble-induced fading exhibiting the most significant impact. Furthermore, the far user's ergodic capacity saturates at high Signal to Noise Ratio (SNR) due to strong interference from the near user. Elamassie et al. [7] extended these findings by evaluating the capacity of multi-user NOMA-enabled UVLC networks and highlighting the trade-offs associated with user pairing and power allocation strategies. To further enhance link reliability, cooperative NOMA frameworks have been proposed, where near users assist far users through relaying, as shown by Kapila et al. in [8], achieving significant gains in coverage and average rate. Moreover, security-oriented studies such as those by Kumar et al. in [9] have investigated NOMA performance under imperfect channel state information, emphasizing the need for robust power-control mechanisms. Although these studies demonstrate the benefits of NOMA in mitigating underwater channel impairments, they largely rely on the assumption of line-of-sight (LOS) transmission. This assumption limits their applicability in realistic underwater environments, where turbulence, scattering, and misalignment frequently disrupt direct optical paths.

On the other hand, IRS has emerged as a transformative technology capable of reshaping the wireless propagation environment. An IRS consists of a planar surface composed of a large number of passive reflecting elements, each capable of independently inducing a controllable phase and/or amplitude shift on the incident signal [10]. In terrestrial optical wireless communication systems, IRS technology has demonstrated significant potential in addressing non-line-of-sight (NLOS) scenarios and improving overall link quality. By intelligently reconfiguring the propagation environment, an IRS can redirect signals toward desired receivers, extend coverage, and mitigate fading effects, thereby substantially enhancing communication reliability and efficiency [11].

Several studies have investigated the integration of IRS into UVLC systems to address key underwater challenges such as signal attenuation, turbulence, and pointing errors. Yalçın Ata et al. [12] analyzed the outage performance of IRS-assisted UVLC links under log-normal turbulence, utilizing the Oceanic Turbulence Optical Power Spectrum model to characterize the underwater medium. Their results reveal that IRS deployment offers significant reliability gains, especially when the number of reflecting elements and the receiver aperture size increase. In a subsequent study [13], Ata et al. introduced a unified channel model for IRS-aided underwater optical wireless communication that incorporates attenuation, turbulence, pointing errors modeled by the Hoyt distribution, and Angle-of-Arrival (AOA) fluctuations. Their analysis, which covers both heterodyne and intensity modulation/direct detection (IM/DD) schemes, confirms the effectiveness of IRS in mitigating combined fading impairments. Focusing on multi-user UVLC scenarios, Rehana Salam et al. in [14] investigated an NLOS configuration using a mirror-array (MA)-based optical IRS. They proposed two mirror allocation strategies—Distance-Based Mirror Assignment (DMA) and Equal Mirror Assignment —and compared their performance with OMA, NOMA, and Rate Split Multiple Access schemes. Their findings indicate that the DMA strategy significantly outperforms alternative approaches in terms of aggregate spectral efficiency and user fairness.

Although NOMA and IRS techniques have independently shown considerable potential in UVLC systems, several important limitations still exist in the current literature. Most NOMA-based UVLC studies mainly consider direct LOS communication and primarily focus on performance metrics such as outage probability, capacity, and BER, without exploring the advantages offered by intelligent signal reflection through IRS technology. Similarly, existing IRS-assisted UVLC research largely emphasizes single-user communication or NLOS enhancement scenarios, while the combined use of IRS and NOMA for multi-user underwater optical communication has not been thoroughly investigated. In addition, the joint effects of underwater turbulence, attenuation, pointing errors, and multi-user interference on IRS–NOMA-enabled UVLC systems have not yet been comprehensively analyzed. Analytical studies addressing key performance measures such as outage probability, coverage probability, and average bit error rate under realistic underwater channel conditions are still limited. Therefore, there is a strong need for an efficient IRS–NOMA-assisted UVLC framework capable of improving communication reliability, spectral efficiency, and user fairness in practical underwater environments. Motivated by these research challenges, this work proposes a novel IRS–NOMA-assisted UVLC framework to improve communication reliability under practical underwater channel impairments. The main contributions of this work are summarized as follows:

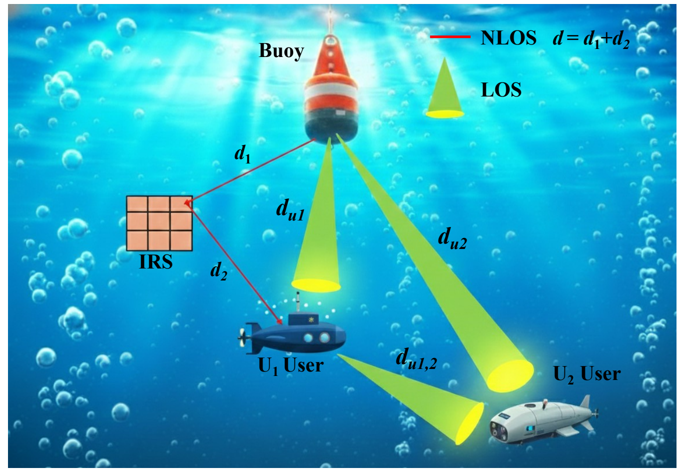

Fig. 1. Proposed IRS-assisted cooperative NOMA-UVLC system model, where a buoy-mounted optical transmitter serves a near user (U_1) and a far user (U_2). The near user receives both direct LOS and IRS-assisted NLOS signals through the reflected path $d = d_1 + d_2$, while the far user receives a direct LOS signal and a cooperative relayed signal from U_1.

- An IRS–NOMA-assisted UVLC system is developed for multi-user underwater optical communication under attenuation, turbulence, and pointing-error effects.
- Closed-form analytical expressions are derived for outage probability, and average bit error rate.
- The influence of IRS reflecting elements, turbulence severity, and pointing misalignment on reliability are examined in detail.
- Numerical and Monte Carlo simulation results are presented to verify the analysis and compare the proposed system with benchmark schemes.

The remainder of this paper is organized as follows. Section II introduces the proposed IRS–NOMA-assisted UVLC system model and describes its key components and operational framework. Section III characterizes the underwater optical channel, including path-loss, pointing errors, and turbulence effects. Section IV develops the analytical expressions for the system performance metrics, namely outage probability, and average bit error rate (ABER). Section V presents and discusses the numerical and simulation results, highlighting the performance gains achieved by the proposed scheme. Finally, Section VI concludes the paper and outlines potential future research directions.

II. Proposed System Model

In this section, we propose a hybrid IRS-assisted NOMA-based UVLC system as shown in Fig. 1. The system consists of a surface buoy acting as the optical base station and two underwater users, namely the near user U_1 located at a distance d_{u_1} and the far user U_2 located at a distance d_{u_2}. An IRS is employed exclusively for assisting the near user and is positioned underwater at a distance d_1 from the buoy and d_2 from U_1.

The buoy transmits optical signals to the users through both LOS and NLOS links. In the LOS link, the optical beam reaches U_1 directly through the channel with coefficient h_1 and reaches U_2 through the channel with coefficient h_2. In the NLOS link, the signal is reflected by the IRS through the channel with coefficient $h_{1,\mathrm{IRS}}$. In addition, U_1 supports cooperative NOMA operation by acting as a decode-and-forward relay[1] for U_2 through the channel with coefficient $h_{1,2}$. The IRS is a passive planar reflecting surface composed of N phase-adjustable mirror elements. From a practical implementation perspective, this configuration can be interpreted as a MEMS-based optical reflector array operating in passive reflection mode, i.e., without signal amplification [15]. By properly tuning these phase shifts, the IRS effectively redirects the optical beam toward the intended user, thereby mitigating underwater impairments such as absorption, scattering, and turbulence. The total propagation distance of the IRS-assisted NLOS path is given by $d = d_1 + d_2$. At the transmitter, the buoy employs superposition coding to generate a composite signal intended for both users, which is expressed as,

$$x(t) = \sqrt{a_1 P_t} X_1 + \sqrt{a_2 P_t} X_2 \quad , \tag{1}$$

where a_1 and a_2 denote the power allocation coefficients assigned to U_1 and U_2, respectively. To ensure feasible decoding under the proposed scheme, the power-allocation coefficients are selected such that $a_1 + a_2 = 1$, $a_2 > a_1$, and the decoding feasibility conditions $a_2 > a_1\gamma_{th,2}$ and $a_1 > \varepsilon a_2 \gamma_{th,1}$ are satisfied. Here, $\gamma_{th,1}$ and $\gamma_{th,2}$ are the threshold to decode the symbols X_1 and X_2, respectively and ε is residual interference. Moreover, P_t represents the total transmit power, X_1 denotes the signal intended for U_1, and X_2 denotes the signal intended for U_2. Accordingly, the signal received at the user is given by,

$$y = \eta x(t) h_{eff} + n_0 \quad , \tag{2}$$

where η denotes the detector responsivity, n_0 represents the Additive White Gaussian Noise (AWGN) with zero mean and variance σ^2, and h_{eff} denotes the effective channel coefficient associated with the LOS, NLOS and relay transmission links. The details of these LOS and NLOS transmission links are presented as follows:

A. LOS Transmission Link:

The LOS transmission takes place between the buoy and user U_i, and the corresponding channel is influenced by three principal impairments, namely path-loss attenuation (h_l), turbulence fading (h_t), and transceiver misalignment (h_p). Therefore, the channel coefficient corresponding to a i^{th} transmission link is given by,

$$h_i = h_{l_i} h_{p_i} h_{t_i}, \tag{3}$$

Using (1), (2), and (3), the received signal at each user U_j is given by,

$$y_{B,U_j} = \eta \left(\sqrt{a_1 P_t} X_1 + \sqrt{a_2 P_t} X_2 \right) h_i + n_0, \quad j \in \{1, 2\}. \tag{4}$$

From (4), the Signal-to-Interference-plus-Noise Ratio (SINR) at user U_1 to decode X_2 symbol is expressed as [16],

$$\gamma_{B,U_1}^{X_2} = \frac{\eta a_2 \rho |h_1|^2}{\eta a_1 \rho |h_1|^2 + 1}, \tag{5}$$

where $\rho = \frac{P_t}{2\sigma^2}$ represents the average SNR. If U_1 successfully decodes the far user's signal X_2, the interference from U_2 can be completely removed through perfect SIC. Otherwise, due to imperfect SIC, a residual interference (ε) remains while decoding the desired signal X_1. Hence, the SINR at U_1 for detecting X_1 is expressed as follows,

$$\gamma_{B,U_1}^{X_1} = \frac{\eta a_1 \rho |h_1|^2}{\eta \varepsilon a_2 \rho |h_1|^2 + 1}, \tag{6}$$

where $\varepsilon = 0$ denotes perfect SIC, while $0 < \varepsilon \leq 1$ represents imperfect SIC. Similarly, the SINR at user U_2 for detecting the symbol X_2 is given by,

$$\gamma_{B,U_2}^{X_2} = \frac{\eta a_2 \rho |h_2|^2}{\eta a_1 \rho |h_2|^2 + 1}. \tag{7}$$

B. NLOS and Relay Transmission Links:

The NLOS transmission takes place between buoy and U_1 through IRS and the relay transmission is between buoy and U_2 through U_1. In the first NLOS link, the channel gain $h_{1,IRS}$ depends on the IRS elements, and is expressed as,

$$h_{1,IRS} = \sum_{n=1}^{N} H_n e^{j\theta_n}, \tag{8}$$

where N denotes the number of reflecting elements in the IRS, and H_n represents the channel gain of the n-th reflecting element, which is given by $H_n = H_{n,d_1} H_{n,d_2}$. Here, $H_{n,d_1} = u_n e^{-j\phi_n}$ denotes the channel gain over the distance d_1 from the buoy to the IRS, while $H_{n,d_2} = v_n e^{-j\psi_n}$ denotes the channel gain over the distance d_2 from the IRS to user U_1. The term $\theta_n \in [0, 2\pi]$ represents the phase shift introduced by the n-th reflecting element. The IRS phase shifts are configured such that $\theta_n = \phi_n + \psi_n$, thereby ensuring constructive signal alignment and maximizing the received SNR [12]. Here ϕ_n and ψ_n are the incident and reflecting angles of the optical beam. We assume perfect continuous phase alignment for analytical tractability, so the obtained IRS gain represents an idealized upper-bound benchmark. Accordingly, phase quantization, practical phase-control errors, underwater perturbations, and misalignment-induced phase mismatches are not explicitly included. Moreover, the analysis is carried

[1] In this paper, it is assumed that the buoy and the relay U_1 operate with the same transmit power.

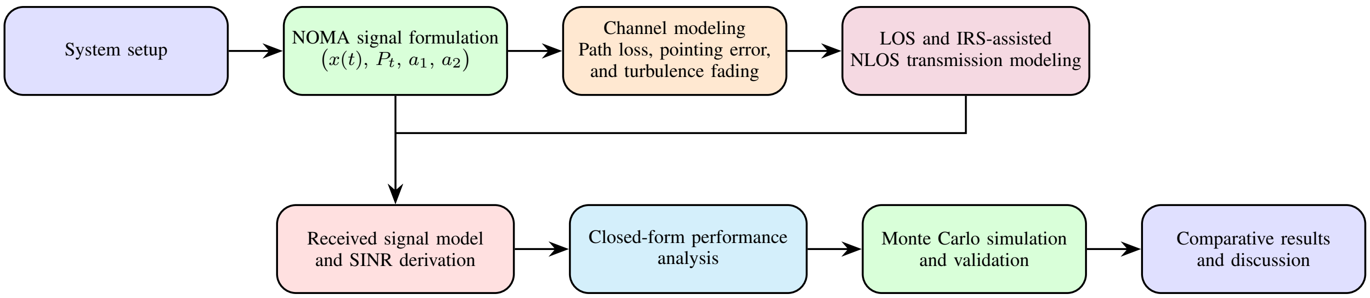

Fig. 2. Methodological workflow of the proposed IRS-assisted NOMA-based UVLC framework.

out under the linear IM/DD regime; therefore, saturation and other higher-order nonlinear effects are neglected.

By substituting this condition into (8), we obtain

$$\begin{aligned} h_{1,IRS} &= \sum_{n=1}^{N} u_n e^{-j\phi_n} v_n e^{-j\psi_n} e^{j\theta_n} \\ &= \sum_{n=1}^{N} u_n v_n = \sum_{n=1}^{N} h_{1,n}. \end{aligned} \tag{9}$$

We assume that all reflecting elements of the IRS are identical, and that the random variables $h_{1,1}, h_{1,2}, \ldots, h_{1,N}$ are independent and identically distributed (i.i.d.). Under this assumption, (9) is simplified as

$$h_{1,IRS} = N h_I, \tag{10}$$

Hence the SINRs at user U_1 to decode both symbols X_2 and X_1 are expressed as

$$\gamma_{U_{1,IRS}}^{X_2} = \frac{\eta a_2 \rho |h_{1,IRS}|^2}{\eta a_1 \rho |h_{1,IRS}|^2 + 1} = \frac{\eta a_2 \rho N^2 |h_I|^2}{\eta a_1 \rho N^2 |h_I|^2 + 1}, \tag{11a}$$

$$\gamma_{U_{1,IRS}}^{X_1} = \frac{\eta a_1 \rho |h_{1,IRS}|^2}{\eta \varepsilon a_2 \rho |h_{1,IRS}|^2 + 1} = \frac{\eta a_1 \rho N^2 |h_I|^2}{\eta \varepsilon a_2 \rho N^2 |h_I|^2 + 1}. \tag{11b}$$

The relay transmission occurs from the buoy to U_2 via U_1, with the corresponding channel coefficient denoted by $h_{1,2}$. The relay link $h_{1,2}$ is modeled in the same manner as h_i, except that its distance parameter corresponds to the U_1–U_2 link. In this case, user U_1 first decodes the symbol intended for U_2 and subsequently forwards it to U_2. Thus, U_1 serves as a relay between the buoy and U_2. Accordingly, the signal received at the far user U_2 is expressed as

$$y_{U_1,U_2} = \eta \sqrt{a_2 P_t} X_2 h_{1,2} + n_0. \tag{12}$$

The corresponding SNRs at user U_2 is given by,

$$\gamma_{U_1,U_2}^{X_2} = \eta a_2 \rho |h_{1,2}|^2. \tag{13}$$

Algorithm 1 summarizes the operation of the proposed IRS-assisted NOMA-based UVLC system. Signal decoding at the users is performed based on the resulting SINR values, with SIC implemented at the near user, while an outage event is declared whenever the required decoding thresholds are not achieved. Fig. 2 depicts the methodological workflow of the proposed IRS-assisted NOMA-based UVLC framework, covering the progression from system modeling to analytical and simulation-based performance evaluation.

Algorithm 1 Proposed IRS-Assisted NOMA-UVLC System with Selection Combining

```
Initialize $P_t$, $N$, $(a_1, a_2)$ with $a_2 > a_1$ target thresholds $(\gamma_{th,1}, \gamma_{th,2})$,
Estimate channel coefficients $h_1$, $h_2$, $h_{1,IRS}$ and $h_{1,2}$;
Compute combined channel gain $h_i = h_{l_i} h_{p_i} h_{t_i}$,  $i \in \{1, 2\}$.;
Compute NOMA signal as $x(t)$ as given by (1);
Compute SINR at $U_1$ and $U_2$ are $\gamma_{B,U_1}^{X_2}$, $\gamma_{B,U_1}^{X_1}$, $\gamma_{B,U_2}^{X_2}$;
Estimate $h_{1,IRS} = \sum_{n=1}^{N} H_{n,d_1} H_{n,d_2} e^{j\theta_n}$;
Reconfigure $\theta_n^\star = \arg(H_{n,d_1}) + \arg(H_{n,d_2})$,  $h_{1,IRS} = \sum_{n=1}^{N} |H_{n,d_1} H_{n,d_2}|$;
Compute $\gamma_{U_{1,IRS}}^{X_2}$, $\gamma_{U_{1,IRS}}^{X_1}$ and $\gamma_{U_1,U_2}^{X_2}$;
Compute $\gamma_{U_1}^{X_2} = \max\left(\gamma_{B,U_1}^{X_2}, \gamma_{U_{1,\text{IRS}}}^{X_2}\right)$, $\gamma_{U_1}^{X_1} = \max\left(\gamma_{B,U_1}^{X_1}, \gamma_{U_{1,\text{IRS}}}^{X_1}\right)$;
Compute $\gamma_{U_2}^{X_2} = max\left\{\min\left(\gamma_{U_1}^{X_2}, \gamma_{U_1,U_2}^{X_2}\right), \gamma_{B,U_2}^{X_2}\right\}$;
if $\gamma_{U_1}^{X_2} < \gamma_{\text{th},2}$ or $\gamma_{U_1}^{X_1} < \gamma_{\text{th},1}$ then
    Compute outage at $U_1$
else
    Successful decoding at $U_1$
end if
if $\gamma_{U_1}^{X_2} < \gamma_{\text{th},2}$ or $\gamma_{U_2}^{X_2} < \gamma_{\text{th},2}$ then
    Compute outage at $U_2$
else
    Successful decoding at $U_2$
end if
```

III. Channel Model

In this section, both users are assumed to operate through UVLC links within the same underwater environment. Hence, they experience similar statistical channel characteristics, although their instantaneous channel gains may differ due to variations in link distance, alignment, and propagation conditions. The overall channel response is modeled by considering three major impairment components: path-loss, transceiver misalignment, and turbulence-induced fading. These components are assumed to be statistically independent for analytical tractability. In addition, the IRS is considered to consist of passive reflecting elements with ideal reflection and perfect phase-adjustment capability. The EGG turbulence model is adopted because of its ability to characterize weak, moderate, and strong underwater turbulence conditions. Its parameters are

TABLE I
EXTINCTION COEFFICIENT IN DIFFERENT WATER MEDIA [15]

Water Type	x_λ	s_λ	e_λ
Pure Sea Water	0.053	0.003	0.056
Clean Ocean Water	0.069	0.081	0.150
Coastal Ocean Water	0.089	0.216	0.305
Turbid Harbor Water	0.295	1.875	2.170

obtained through statistical fitting of experimentally observed irradiance fluctuations under different underwater turbulence conditions.

A. Path-Loss channel coefficient

According to the Beer–Lambert law, the path-loss in UVLC systems is primarily governed by absorption and scattering effects. This attenuation can be expressed as [12]

$$h_l = exp(-e_\lambda L), \tag{14}$$

where e_λ denotes the extinction coefficient, defined as the sum of the absorption coefficient x_λ and the scattering coefficient s_λ, i.e., $e_\lambda = x_\lambda + s_\lambda$. The value of e_λ varies for different water types, as summarized in Table I [15]. Here, L represents the transmission link distance.

B. Pointing Error Channel Coefficient

In LOS communication systems, pointing accuracy plays a crucial role in maintaining reliable link performance. Misalignment often occurs due to factors such as wind loads, thermal expansion, water currents, and tidal variations, which cause displacement between the transmitter and receiver. Pointing errors are typically classified into two types: boresight error, representing a constant offset between the beam and the detector center, and jitter variance, denoting the random fluctuations of the beam spot [17].

In UVLC systems, these impairments are further intensified by underwater environmental dynamics, including ocean currents, surface waves, relay buoy tilting, and thermal variations. Such misalignments lead to fluctuations in the received optical power, introducing an additional fading component that degrades overall system performance. Therefore, robust pointing, acquisition, and tracking mechanisms are essential for ensuring stable communication in harsh underwater conditions. The pointing error channel is typically modeled using a Rayleigh distribution and is expressed as [17]

$$f_{h_p}(h_p) = \frac{\zeta^2}{A_p^{\zeta^2}} h_p^{\zeta^2-1}, \quad 0 \le h_p \le A_p \tag{15}$$

where $\zeta = \frac{\omega_{z_{eq}}}{2\sigma_p}$ denotes the ratio between the equivalent beam radius $\omega_{z_{eq}}$ and the standard deviation σ_p of the pointing error displacement at both transmitter and receiver ends. The equivalent beam radius is $\omega_{z_{eq}} = w_z\sqrt{\frac{\sqrt{\pi}erf(v)}{2vexp(-v^2)}}$, where $v = \sqrt{\frac{\pi}{2}}\frac{D_R}{w_z}$ represents the ratio between the receiver aperture radius A_R and the beam width $w_z = w_0\sqrt{1+(\frac{\lambda z}{\pi w_0^2})^2}$. Here, w_0 is the spot size of the Gaussian beam wave and λ is the transmission light wavelength. The parameter A_p is defined as $A_p = [erf(v)]^2$.

C. Turbulence Channel Fading Model

In UVLC systems, turbulence arises from random fluctuations in temperature, density, salinity, and pressure within the underwater environment. These fluctuations induce stochastic variations in the refractive index, which in turn cause intensity fading at the receiver. To accurately model this behavior, we employ the EGG distribution, a mixture model that combines the Exponential and Generalized Gamma distributions through a weighted sum [20]. For the convenience of the reader, Table II summarizes the differences between the proposed framework and related studies in terms of system configuration, adopted channel model, and main contribution. Unlike the existing studies summarized in Table II, the proposed framework jointly considers IRS-assisted propagation, NOMA-based multi-user transmission, pointing errors, and EGG turbulence fading within a unified analytical framework. The PDF of the turbulence-induced fading coefficient is expressed as

$$\begin{aligned} f_{h_t}(h_t) =& \frac{\omega}{\lambda}\exp\left(-\frac{h_t}{\lambda}\right) + \\ & \frac{c(1-\omega)}{b^{ac}\Gamma(a)} h_t^{ac-1} \exp\left[-\left(\frac{h_t}{b}\right)^c\right], \end{aligned} \tag{16}$$

where ω is the mixture coefficient satisfying $0 < \omega < 1$, λ is the exponential distribution parameter, and a, b, and c denote the generalized gamma parameters. Here, $\Gamma(\cdot)$ represents the gamma function. It should be noted that the EGG parameter set $(\omega, \lambda, a, b, c)$ is condition-dependent and is obtained through statistical fitting to measured irradiance data for each specific turbulence scenario [20]. Therefore, the cited model does not provide an explicit closed-form mapping from bubble level (BL) to the corresponding EGG parameters. Moreover, ω represents the mixture weight of the exponential component and may be physically interpreted as the relative contribution of bubble-dominated deep-fading events in the overall UWOC turbulence statistics.

D. Combined Channel Gain

We assume that both users experience nearly identical underwater channel impairments. Thus, the combined normalized channel gain for user i is modeled as the product of the independent fading components:

$$h_i = h_{l_i} h_{p_i} h_{t_i}, \tag{17}$$

Considering turbulenceh_{t_i}, pointing errorsh_{p_i}, and deterministic attenuation jointly, (17) can be expressed as,

$$\frac{h_i}{h_{l_i}} = h_{p_i} h_{t_i}, \tag{18}$$

Since h_{p_i} and h_{t_i} are random variables, the PDF of the combined channel gain is obtained using the transformation of random variables [12]:

$$f_{h_i}(h_i) = \int f_{h_i/h_{t_i}}\left(\frac{h_i}{h_{t_i}}\right) f_{h_{t_i}}(h_{t_i}) \quad dh_t, \tag{19}$$

TABLE II
COMPARISON OF THE POPOSED FRAMEWORK WITH RELATED WORKS IN TERMS OF SYSTEM MODEL, CHANNEL MODEL, AND MAIN CONTRIBUTION

Reference	System Type	Fading / Channel Model	IRS	NOMA	Main Contribution	Performance Metrics
[12]	UVLC system	Log-normal	Yes	No	IRS-assisted UVLC performance analysis	Outage probability
[18]	UVLC system	EGG model	No	Yes	NOMA-based UVLC with EGG fading analysis	Outage probability
[16]	Full-duplex UVLC system	EGG model	No	Yes	Cooperative/full-duplex NOMA-UVLC framework	Outage probability, coverage probability
[19]	UWOC system	Gamma–Gamma	Yes	No	IRS-assisted UWOC performance analysis	Outage probability, ergodic capacity
Proposed Scheme	IRS-assisted NOMA-UVLC system	EGG model	Yes	Yes	Joint integration of IRS and NOMA for UVLC under EGG turbulence	Outage probability, BER, coverage probability

where the conditional PDF is valid for $0 \leq h_i \leq A_p h_{l_i} h_{t_i}$.

$$f_{h_i/h_{t_i}}\left(\frac{h_i}{h_{t_i}}\right) = \frac{1}{h_{l_i}h_{t_i}} f_{h_p}\left(\frac{h_i}{h_{l_i}h_t}\right) = \frac{\zeta^2}{A_p^{\zeta^2} h_{l_i}h_{t_i}}\left(\frac{h_i}{h_{l_i}h_{t_i}}\right)^{\zeta^2-1}, \tag{20}$$

Substituting (16) and (20) into (19), we obtain

$$f_{h_i}(h_i) = \int_{\frac{h_i}{A_p h_{l_i}}}^{\infty} \frac{\zeta^2}{A_p^{\zeta^2} h_{l_i}h_{t_i}}\left(\frac{h_i}{h_{l_i}h_{t_i}}\right)^{\zeta^2-1} \times \left[\frac{\omega}{\lambda}\exp\left(-\frac{h_{t_i}}{\lambda}\right) + \frac{c(1-\omega)}{b^{ac}\,\Gamma(a)} h_{t_i}^{ac-1}\exp\left[-\left(\frac{h_{t_i}}{b}\right)^c\right]\right] dh_{t_i}. \tag{21}$$

Since the composite channel satisfies $h_i = h_{l_i} h_p h_{t_i}$ and the pointing error coefficient is bounded as $0 \leq h_p \leq A_p$, it follows that $h_i \leq A_p h_{l_i} h_{t_i}$, which yields $h_{t_i} \geq \frac{h_i}{A_p h_{l_i}}$. Hence, the lower limit of the integral with respect to h_{t_i} is $\frac{h_i}{A_p h_{l_i}}$. We evaluate the integral by separating it into two terms, denoted by Π_0 and Π_1. Hence

$$f_{h_i}(h_i) = \Pi_0 + \Pi_1 \tag{22}$$

$$\Pi_0 = \int_{\frac{h_i}{A_p h_{l_i}}}^{\infty} \frac{\zeta^2}{A_p^{\zeta^2} h_{l_i}h_{t_i}}\left(\frac{h_i}{h_{l_i}h_{t_i}}\right)^{\zeta^2-1} \frac{\omega}{\lambda}\exp\left(-\frac{h_{t_i}}{\lambda}\right) dh_{t_i} = \frac{\omega\zeta^2 h_i^{\zeta^2-1}}{\lambda A_p^{\zeta^2} h_{l_i}^{\zeta^2}} \int_{\frac{h_i}{A_p h_{l_i}}}^{\infty} \frac{1}{h_{t_i}^{\zeta^2}}\exp\left(-\frac{h_{t_i}}{\lambda}\right) dh_{t_i}. \tag{23}$$

Comparing (23) with (3) of Section 3.381 in [21], $\int_u^\infty x^{\nu-1}e^{-\mu x}\,dx = \mu^{-\nu}\Gamma(\nu,\mu u)$, and setting $u = \frac{h_i}{A_p h_{l_i}}$, $\nu = 1-\zeta^2$, and $\mu = \frac{1}{\lambda}$, (23) can be expressed as follows:

$$\Pi_0 = \frac{\omega\zeta^2 h_i^{\zeta^2-1}}{(A_p h_{l_i}\lambda)^{\zeta^2}}\Gamma\left(1-\zeta^2, \frac{h_i}{A_p h_{l_i}\lambda}\right). \tag{24}$$

Similarly, for Π_1,

$$\Pi_1 = \int_{\frac{h_i}{A_p h_{l_i}}}^{\infty} \frac{\zeta^2}{A_p^{\zeta^2} h_{l_i}h_{t_i}}\left(\frac{h_i}{h_{l_i}h_{t_i}}\right)^{\zeta^2-1} \times \frac{c(1-\omega)}{b^{ac}\Gamma(a)} h_{t_i}^{ac-1} exp\left[-\left(\frac{h_{t_i}}{b}\right)^c\right] dh_{t_i}, = \frac{c(1-\omega)\zeta^2 h_i^{\zeta^2-1}}{b^{ac}\Gamma(a) A_p^{\zeta^2} h_{l_i}^{\zeta^2}} \int_{\frac{h_i}{A_p h_{l_i}}}^{\infty} h_{t_i}^{ac-1-\zeta^2} exp\left[-\left(\frac{h_{t_i}}{b}\right)^c\right] dh_{t_i}. \tag{25}$$

Comparing (25) with (9) of Section 3.381 in [21], $\int_u^\infty x^m e^{-\beta x^n}\,dx = \frac{\Gamma(\nu,\beta u^n)}{n\beta^\nu}$, $\nu = \frac{m+1}{n}$, and setting $u = \frac{h_i}{A_p h_{l_i}}$, $m = ac-1-\zeta^2$, $\beta = \frac{1}{b^c}$, $n = c$, and $\nu = \frac{m+1}{n}$, (25) can be written as follows:

$$\Pi_1 = \frac{(1-\omega)\zeta^2 h_i^{\zeta^2-1}}{(A_p h_{l_i} b)^{\zeta^2}\quad\Gamma(a)}\Gamma\left[a-\frac{\zeta^2}{c}, \left(\frac{h_i}{A_p h_{l_i} b}\right)^c\right]. \tag{26}$$

Substituting (24) and (26) into (22), the PDF expression in Eq. (23) is obtained as,

$$f_{h_i}(h_i) = \frac{\zeta^2 h_i^{\zeta^2-1}}{(A_p h_{l_i})^{\zeta^2}}\left[\frac{\omega}{\lambda^{\zeta^2}}\Gamma\left(1-\zeta^2, \frac{h_i}{A_p h_{l_i}\lambda}\right) + \frac{1-\omega}{\Gamma(a) b^{\zeta^2}}\Gamma\left(a-\frac{\zeta^2}{c}, \left(\frac{h_i}{A_p h_{l_i} b}\right)^c\right)\right]. \tag{27}$$

Further, rewriting (27) in terms of Meijer-G functions using (07.34.03.0613.01) in [22], we obtain

$$f_{h_i}(h_i) = \frac{\zeta^2 h_i^{\zeta^2-1}}{(A_p h_{l_i})^{\zeta^2}}\left[\frac{\omega}{\lambda^{\zeta^2}} G_{1,2}^{2,0}\left(\frac{h_i}{A_p h_{l_i}\lambda}\,\middle|\, \begin{matrix} 1 \\ 1-\zeta^2,\, 0 \end{matrix}\right) + \frac{1-\omega}{\Gamma(a) b^{\zeta^2}} G_{1,2}^{2,0}\left(\left(\frac{h_i}{A_p h_{l_i} b}\right)^c \,\middle|\, \begin{matrix} 1 \\ a-\frac{\zeta^2}{c},\, 0 \end{matrix}\right)\right]. \tag{28}$$

The CDF corresponding to the above PDF is given by,

$$F_{h_i}(h_i) = \int_0^{h_i} f_{h_i}(h_i) dh_i, \tag{29}$$

Using (07.34.21.0003.01) in [22], the CDF can be expressed as (30).

$$F_{h_i}(h_i) = \zeta^2 \left(\frac{h_i}{A_p h_{l_i}}\right)^{\zeta^2} \times \left[\frac{\omega}{\lambda\zeta^2} G_{2,3}^{2,1}\left(\frac{h_i}{A_p h_{l_i}\lambda} \middle| \begin{array}{c} 1-\zeta^2, 1 \\ 1-\zeta^2, 0, -\zeta^2 \end{array}\right) + \frac{1-w}{c\Gamma(a) b^{\zeta^2}} G_{2,3}^{2,1}\left(\left(\frac{h_i}{A_p h_{l_i} b}\right)^c \middle| \begin{array}{c} 1-\frac{\zeta^2}{c}, 1 \\ a-\frac{\zeta^2}{c}, 0, -\frac{\zeta^2}{c} \end{array}\right)\right]. \quad (30)$$

IV. Performance Analysis

In this section, we evaluate the performance of the proposed system in terms of outage probability, and ABER. These metrics are widely adopted in UVLC and related optical wireless systems, as they provide insight into the robustness of the link under various channel impairments. The outage probability characterizes the likelihood that the system fails to meet a predefined SNR threshold, whereas the average BER quantifies the probability of incorrect bit detection at the receiver. Taken together, these metrics offer a comprehensive view of the system's reliability and data integrity.

A. Outage Probability

Outage probability is a key metric for assessing the reliability of a communication system under fading and noise. It is defined as the probability that the instantaneous received SNR $\gamma_{U_i}^{X_i}$ falls below the target SNR threshold γ_{th_i}, where $\gamma_{th_i} = 2^{R_{U_i}^{X_i}} - 1$ is the minimum SNR required to support the desired data rate $R_{U_i}^{X_i}$.

1) Outage Probability of Near User: An outage event at user U_1 is declared when the required signals cannot be successfully decoded through either the LOS or the NLOS transmission path under selection combining. Therefore, the outage probability at U_1 is given by,

$$\begin{aligned} P_{out,U_1} &= \Pr[\max\left(\gamma_{U_1}^{LOS}, \gamma_{U_1}^{NLOS}\right) < \gamma_{th,i}] \\ &= \Pr(\gamma_{U_1}^{LOS} < \gamma_{th,i}, \quad \gamma_{U_1}^{NLOS} < \gamma_{th,i}) \\ &= P_{out,U_1}^{LOS} P_{out,U_1}^{NLOS} \end{aligned} \quad (31)$$

Here, $\gamma_{th,i}$ is a threshold for decoding the symbol X_i intended for a user. Moreover, the outage event at the user U_1 is defined as the failure to decode X_2 or X_1 through a given LOS or NLOS transmission path. Therefore, the outage probability of U_1 corresponding to each transmission path can be expressed as,

$$P_{out,U_1}^{LOS} = \Pr[\gamma_{B,U_1}^{X_2} < \gamma_{th,2} \text{ or } \gamma_{B,U_1}^{X_1} < \gamma_{th,1}], \quad (32a)$$

$$P_{out,U_1}^{NLOS} = \Pr[\gamma_{U_1,IRS}^{X_2} < \gamma_{th,2} \text{ or } \gamma_{U_1,IRS}^{X_1} < \gamma_{th,1}]. \quad (32b)$$

From (5), we obtain $h_1 < \alpha_1$, where $\alpha_1 = \frac{\gamma_{th,2}}{\eta\rho(a_2 - a_1\gamma_{th,2})}$ and from (6), we obtain $h_1 < \beta_1$, where $\beta_1 = \frac{\gamma_{th,1}}{\eta\rho(a_1 - a_2\varepsilon\gamma_{th,1})}$. Hence, (32a) becomes

$$P_{out,U_1}^{LOS} = \Pr[h_1 < \alpha_1 \text{ or } h_1 < \beta_1] = \Pr(h_1 < \Delta_1) = F_{h_1}(\Delta_1), \quad (33)$$

where $\Delta_1 = \max(\alpha_1, \beta_1)$. Similarly, from (11a), we get $h_I < \alpha_{1,IRS}$ where $\alpha_{1,IRS} = \frac{\gamma_{th,2}}{\eta\rho(a_2 - a_1\gamma_{th,2})N^2}$ and from (11b), we obtain $h_I < \beta_{1,IRS}$, where $\beta_{1,IRS} = \frac{\gamma_{th,1}}{\eta\rho(a_1 - a_2\varepsilon\gamma_{th,1})N^2}$. Hence, (32b) becomes

$$\begin{aligned} P_{out,U_1}^{NLOS} &= \Pr[h_{1,IRS} < \alpha_{1,IRS} \text{ or } h_{1,IRS} < \beta_{1,IRS}] \\ &= \Pr(h_{1,IRS} < \Delta_{1,IRS}) = F_{h_{1,IRS}}(\Delta_{1,IRS}), \end{aligned} \quad (34)$$

where $\Delta_{1,IRS} = \max(\alpha_{1,IRS}, \beta_{1,IRS})$. Hence 31 becomes as

$$P_{out,U_1} = F_{h_1}(\Delta_1) F_{h_{1,IRS}}(\Delta_{1,IRS}), \quad (35)$$

2) Outage Probability of Far User: The signals received at U_2 through the LOS and user-relayed paths are combined using selection combining. Accordingly, the resulting SINR at U_2, denoted by $\gamma_{U_2}^{X_2}$, is given by [16].

$$\gamma_{U_2}^{X_2} = max\left\{\min\left(\gamma_{U_1}^{X_2}, \gamma_{U_1,U_2}^{X_2}\right), \gamma_{B,U_2}^{X_2}\right\}. \quad (36)$$

An outage event at user U_2 occurs when it fails to decode X_2. Thus, the outage probability at U_2 is given by

$$P_{out,U_2} = \Pr[\gamma_{U_2}^{X_2} < \gamma_{th,2}], \quad (37)$$

Since the channels are independent, it can be rewritten as [16]

$$\begin{aligned} P_{out,U_2} &= \Pr\left\{\min\left(\gamma_{U_1}^{X_2}, \gamma_{U_1,U_2}^{X_2}\right) \le \gamma_{th,2}\right\} \times \Pr\left\{\gamma_{B,U_2}^{X_2} \le \gamma_{th,2}\right\} \\ &= \Big[1 - \underbrace{\Pr\left(\gamma_{U_1}^{X_2} > \gamma_{th,2}\right)}_{\text{Term-P}_1^{U_2}} \underbrace{\Pr\left(\gamma_{U_1,U_2}^{X_2} > \gamma_{th,2}\right)}_{\text{Term-P}_2^{U_2}}\Big] \times \underbrace{\Pr\left\{\gamma_{B,U_2}^{X_2} \le \gamma_{th,2}\right\}}_{\text{Term-P}_3^{U_2}}. \end{aligned} \quad (38)$$

Consider Term-$\text{P}_1^{U_2}$, and it can be simplified as,

$$\begin{aligned} \text{Term-P}_1^{U_2} &= \Pr\left(\gamma_{U_1}^{X_2} > \gamma_{th,2}\right) \\ &= 1 - \Pr\left(\gamma_{U_1}^{X_2} < \gamma_{th,2}\right) \\ &= 1 - \Pr\left(\max\left\{\gamma_{B,U_1}^{X_2}, \gamma_{U_1,IRS}^{X_2}\right\} < \gamma_{th,2}\right) \\ &= 1 - \left[\Pr\left(\gamma_{B,U_1}^{X_2} < \gamma_{th,2} \quad , \quad \gamma_{U_1,IRS}^{X_2} < \gamma_{th,2}\right)\right] \\ &= 1 - \left[\Pr\left(h_1 < \alpha_1 \quad , \quad h_{1,IRS} < \alpha_{1,IRS}\right)\right] \\ &= 1 - \left[F_{h_1}(\alpha_1) F_{h_{1,IRS}}(\alpha_{1,IRS})\right] \end{aligned} \quad (39)$$

Consider Term-$\text{P}_2^{U_2}$, and it can be simplified as,

$$\begin{aligned} \text{Term-P}_2^{U_2} &= \Pr\left(\gamma_{U_1,U_2}^{X_2} > \gamma_{th,2}\right) \\ &= 1 - \Pr\left(\gamma_{U_1,U_2}^{X_2} < \gamma_{th,2}\right) \\ &= 1 - F_{h_{1,2}}(\alpha_{1,2}), \end{aligned} \quad (40)$$

From (13), $h_{1,2} < \alpha_{1,2}$, where $\alpha_{1,2} = \frac{\gamma_{th,2}}{\eta\rho a_2}$

Consider Term-$\text{P}_3^{U_2}$, and it can be simplified as,

$$\begin{aligned} \text{Term-P}_3^{U_2} &= \Pr\left(\gamma_{B,U_2}^{X_2} < \gamma_{th,2}\right) \\ &= \Pr\left(h_2 < \alpha_2\right) = F_{h_2}(\alpha_2), \end{aligned} \quad (41)$$

From (7), $h_2 < \alpha_2$ where $\alpha_2 = \frac{\gamma_{th,2}}{\eta\rho(a_2 - a_1\gamma_{th,2})}$. Hence the (37) becomes

$$P_{out,U_2} = \Big[1 - \big(1 - F_{h_1}(\alpha_1)F_{h_{1,\mathrm{IRS}}}(\alpha_{1,\mathrm{IRS}})\big) \big(1 - F_{h_{1,2}}(\alpha_{1,2})\big)\Big] F_{h_2}(\alpha_2). \quad (42)$$

The system outage probability is defined as the probability that at least one of the users U_1 or U_2 experiences an outage. It is expressed as

$$P_{out}^{sys} = 1 - [(1 - P_{out,U_1})(1 - P_{out,U_2})]. \quad (43)$$

B. Average Bit Error Rate

The average bit error rate (ABER) represents the long-term probability of erroneous bit detection at the receiver and serves as an important measure of the reliability of the proposed IRS-assisted cooperative NOMA-UVLC framework. In underwater optical channels, the ABER is strongly affected by deterministic attenuation, turbulence-induced fading, pointing errors, and the cooperative transmission strategy. In this work, On–Off Keying (OOK) modulation is considered due to its low implementation complexity and suitability for intensity-modulated optical communication systems.

For OOK signaling, the ABER of user U_i can be expressed as

$$\overline{P}_{b,U_i} = \int_0^\infty Q\left(\sqrt{\frac{\gamma_{U_i}^{\mathrm{eff}}}{2}}\right) f_{\gamma_{U_i}^{\mathrm{eff}}}(\gamma)\, d\gamma, \quad (44)$$

where $Q(\cdot)$ denotes the Gaussian Q-function and $\gamma_{U_i}^{\mathrm{eff}}$ is the effective instantaneous SINR at user U_i.

In the proposed framework, the near user U_1 receives the desired signal through both the direct LOS branch and the IRS-assisted branch. Under selection combining, the effective SINR at U_1 is given by

$$\gamma_{U_1}^{\mathrm{eff}} = \max\left(\gamma_{U_1}^{\mathrm{LOS}}, \gamma_{U_1}^{\mathrm{NLOS}}\right). \quad (45)$$

Hence, the corresponding CDF is

$$F_{\gamma_{U_1}^{\mathrm{eff}}}(\gamma) = F_{\gamma_{U_1}^{\mathrm{LOS}}}(\gamma)\, F_{\gamma_{U_1}^{\mathrm{IRS}}}(\gamma), \quad (46)$$

and the PDF is obtained as

$$f_{\gamma_{U_1}^{\mathrm{eff}}}(\gamma) = f_{\gamma_{U_1}^{\mathrm{LOS}}}(\gamma)\, F_{\gamma_{U_1}^{\mathrm{NLOS}}}(\gamma) + f_{\gamma_{U_1}^{\mathrm{NLOS}}}(\gamma)\, F_{\gamma_{U_1}^{\mathrm{LOS}}}(\gamma). \quad (47)$$

For the far user U_2, reception is achieved through cooperative transmission. Specifically, U_1 first decodes the symbol intended for U_2 and then forwards it over the relay link. The end-to-end relay-path SINR is therefore expressed as

$$\gamma_{R,U_2} = \min\left(\gamma_{x_2,U_1}^{\mathrm{eff}}, \gamma_{U_1U_2}\right), \quad (48)$$

where

$$\gamma_{x_2,U_1}^{\mathrm{eff}} = \max\left(\gamma_{x_2,U_1}^{\mathrm{LOS}}, \gamma_{x_2,U_1}^{\mathrm{IRS}}\right) \quad (49)$$

denotes the effective SINR for decoding x_2 at U_1. Accordingly, the CDF of the relay-path SINR is written as

$$F_{\gamma_{R,U_2}}(\gamma) = 1 - \left[1 - F_{\gamma_{x_2,U_1}^{\mathrm{eff}}}(\gamma)\right]\left[1 - F_{\gamma_{U_1U_2}}(\gamma)\right]. \quad (50)$$

Since U_2 also receives the direct signal from the buoy, the effective SINR at U_2 under selection combining is

$$\gamma_{U_2}^{\mathrm{eff}} = \max\left(\gamma_{BU_2}, \gamma_{R,U_2}\right), \quad (51)$$

which yields the CDF

$$F_{\gamma_{U_2}^{\mathrm{eff}}}(\gamma) = F_{\gamma_{BU_2}}(\gamma)\, F_{\gamma_{R,U_2}}(\gamma), \quad (52)$$

and the corresponding PDF

$$f_{\gamma_{U_2}^{\mathrm{eff}}}(\gamma) = f_{\gamma_{BU_2}}(\gamma)\, F_{\gamma_{R,U_2}}(\gamma) + f_{\gamma_{R,U_2}}(\gamma)\, F_{\gamma_{BU_2}}(\gamma). \quad (53)$$

Substituting (47) and (53) into (44), the ABER of U_1 and U_2 can be respectively expressed as

$$\overline{P}_{b,U_1} = \int_0^\infty Q\left(\sqrt{\frac{\gamma}{2}}\right) f_{\gamma_{U_1}^{\mathrm{eff}}}(\gamma)\, d\gamma, \quad (54)$$

and

$$\overline{P}_{b,U_2} = \int_0^\infty Q\left(\sqrt{\frac{\gamma}{2}}\right) f_{\gamma_{U_2}^{\mathrm{eff}}}(\gamma)\, d\gamma. \quad (55)$$

V. Results and Discussion

This section presents the numerical results of the proposed IRS-assisted NOMA-UVLC system. The performance evaluation is conducted using various underwater channel parameters, with the corresponding numerical values summarized in Table III. The specific EGG distribution parameters associated with different bubble lengths (BLs) for both saltwater and freshwater are listed in Table IV. All the analytical expressions are validated by Monte Carlo simulations. For Monte Carlo validation, each simulated point is obtained using 10^5 independent channel realizations. The turbulence-induced fading coefficient is generated according to the EGG model using a mixture-based sampling procedure. Specifically, for each realization, a uniform random variable is generated to select the exponential distribution with probability ω or the generalized-gamma distribution with probability $1-\omega$. If the exponential distribution is selected, the sample is generated from an exponential distribution with parameter λ. Otherwise, a Gamma random variable $Y \sim \Gamma(a, 1)$ is first generated, and the corresponding generalized-gamma sample is obtained as $h_{t_i} = bY^{1/c}$. The pointing error coefficients are generated independently for each realization according to the adopted pointing error model. Moreover, under the ideal phase-control assumption, the IRS phase shifts are updated once per channel realization to ensure constructive signal alignment.

Furthermore, the robustness of the proposed IRS-assisted NOMA in UVLC system is examined by analyzing the effect of key design and channel parameters on the outage performance. Specifically, the influence of the number of IRS reflecting elements N, NOMA power allocation coefficient a_2, bubble level (BL), and pointing-error parameter ζ is considered. These parameters are important because they affect the reflected link gain, power distribution among users, turbulence-induced fading, and alignment accuracy, respectively. The corresponding results provide useful design insights into the behavior of the proposed system under practical underwater channel variations.

TABLE III
PARAMETERS CONSIDERED FOR NUMERICAL RESULTS

Parameter	Value	Parameter	Value
η	0.9	R	1cm
ϵ	0.01	w_0	1cm
λ	470nm	a_1	0.3
D_R	5cm	a_2	0.7

TABLE IV
PARAMETERS OF EGG DISTRIBUTION[20]

Water type	B.L (L/min)	ω	λ	a	b	c
Salt water	4.7	0.2064	0.3953	0.5307	1.2154	35.7368
Salt water	16.5	0.4951	0.1368	0.0161	3.2033	82.1030
Fresh water	4.7	0.2109	0.4603	1.2526	1.1501	41.3258
Fresh water	16.5	0.5117	0.1602	0.0075	2.9963	216.8356

A. Outage Probability vs SNR

To benchmark the proposed framework against representative baseline schemes reported in the literature, Table V compares the outage performance of conventional NOMA without IRS, inspired by [18], and cooperative NOMA (CNOMA) without IRS, inspired by [16], with that of the proposed IRS-assisted NOMA scheme under the same simulation settings for $\mathrm{BL} = 4.7$ L/min.

As shown in Table V, the outage probability of all schemes decreases with increasing SNR, due to the fact that a higher received SINR improves the probability of successful decoding. Among the considered schemes, the proposed IRS-assisted NOMA framework consistently achieves the lowest outage probability for both users, thereby demonstrating a clear reliability advantage over the benchmark schemes adopted from [18] and [16]. In particular, for the near user U_1, the proposed scheme reduces the outage probability from 2.5×10^{-7} at 50 dB to 2.0×10^{-9} at 60 dB, which is significantly lower than the corresponding values of the conventional NOMA baseline in [18] and the CNOMA baseline in [16]. This behavior can be attributed to the IRS-enhanced reflected link, which improves the effective channel quality and reduces the probability that the instantaneous SINR falls below the target threshold. Overall, the quantitative results in Table V show that the proposed IRS-assisted NOMA framework significantly improves system reliability compared with the benchmark schemes. At $\mathrm{SNR} = 60$ dB, the proposed scheme achieves an outage probability for U_1 that is approximately two orders of magnitude lower than conventional NOMA and seven orders of magnitude lower than CNOMA. Similarly, for U_2, the proposed framework provides nearly one order of magnitude improvement over conventional NOMA and more than three orders of magnitude improvement over CNOMA. These results confirm the effectiveness of IRS-assisted signal enhancement in improving underwater communication reliability.

The outage probability, P_{out}, as a function of SNR for the proposed system is presented in Fig. 3, which also includes the corresponding performance of the system without IRS for comparison. In accordance with theoretical expectations, the outage probability decreases with increasing SNR, since a higher received SINR increases the probability that the decoding threshold is successfully satisfied. It is evident from the figure that the incorporation of IRS yields a substantial reduction in outage probability, thereby confirming its effectiveness in enhancing the effective channel quality through intelligent signal reflection. In particular, at an SNR of 25 dB, the outage probability of U_1 in the IRS-assisted case falls below 10^{-2}, whereas the corresponding value for the non-IRS case remains above 10^{-1}. For the far user U_2, the outage probability is observed to be approximately 10^{-1}, indicating that although this user remains subject to comparatively less favorable transmission conditions, the proposed framework still provides a meaningful reliability improvement. These results demonstrate that the deployment of IRS significantly mitigates the probability of decoding failure and, consequently, enhances the overall communication reliability of the considered system.

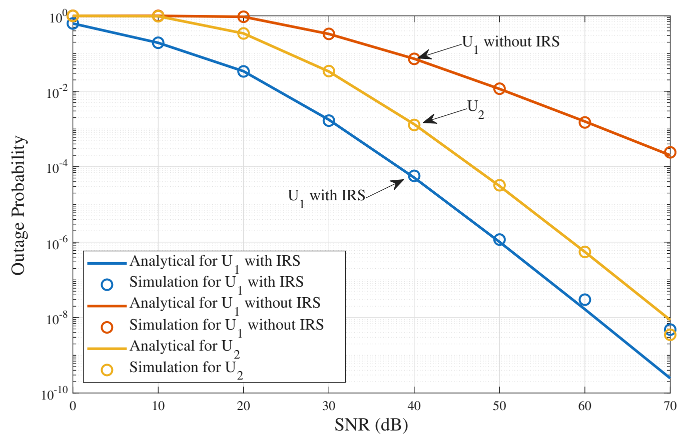

Fig. 3. Outage Probability of U_1 user with and without IRS and U_2 user.

Fig.4 illustrates the sensitivity of the user outage performance to the power-allocation coefficient a_2. The results show

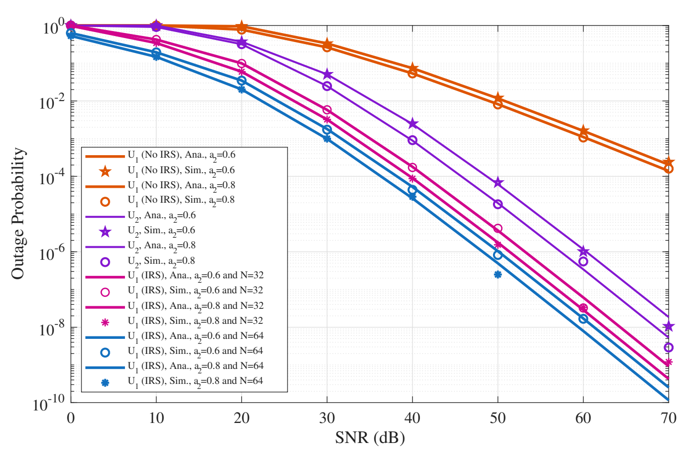

Fig. 4. Outage probability comparison of U_1 and U_2 under different power-allocation settings a_2, illustrating the parameter-sensitive fairness behavior of the proposed scheme in both IRS-assisted and non-IRS scenarios.

TABLE V
COMPARISON OF OUTAGE PROBABILITY FOR CONVENTIONAL NOMA AND COOPERATIVE NOMA BASELINE SCHEMES, INSPIRED BY [18] AND [16], AND THE PROPOSED IRS-ASSISTED NOMA SCHEME UNDER THE SAME SIMULATION SETTINGS FOR BL = 4.7 L/MIN

SNR in	NOMA without IRS [18]		CNOMA without IRS [16]		Proposed Scheme	
dB	U_1	U_2	U_1	U_2	U_1	U_2
50	3.0×10^{-6}	2.0×10^{-5}	7.0×10^{-2}	2.4×10^{-3}	2.5×10^{-7}	1.5×10^{-5}
55	8.0×10^{-7}	1.1×10^{-5}	3.7×10^{-2}	1.3×10^{-3}	2.2×10^{-8}	1.7×10^{-6}
60	2.5×10^{-7}	6.5×10^{-6}	2.0×10^{-2}	7.0×10^{-4}	2.0×10^{-9}	2.0×10^{-7}
65	3.5×10^{-8}	5.0×10^{-7}	1.2×10^{-2}	4.0×10^{-4}	8.0×10^{-10}	2.8×10^{-8}
70	4.5×10^{-9}	2.5×10^{-8}	7.0×10^{-3}	2.2×10^{-4}	3.0×10^{-11}	4.0×10^{-9}

that the relative performance of U_1 and U_2 is not fixed, but depends strongly on the system configuration. In the non-IRS case, U_2 benefits from both the direct transmission from the buoy and the relayed transmission through U_1, and therefore achieves a lower outage probability than U_1 for certain power-allocation settings, such as $a_2 = 0.6$ and $a_2 = 0.8$. In contrast, when IRS assistance is introduced, the passive beamforming gain significantly strengthens the effective channel of U_1, causing the performance order to reverse such that U_1 outperforms U_2. This behavior confirms that fairness in the proposed system is parameter-sensitive and governed by the tradeoff between IRS beamforming gain and NOMA power allocation, rather than being an inherent property of the architecture.

Figs. 5, 6, and 7 collectively characterize the outage performance of the proposed system under variations in the number of IRS reflecting elements N, the target SINR threshold γ_{th}, and the pointing error parameter ζ. From a theoretical perspective, increasing N is expected to improve the passive beamforming capability of the IRS, thereby enhancing the effective channel gain and reducing the outage probability. This expected behavior is clearly observed in Fig. 5, where larger values of N result in a pronounced improvement in reliability. By contrast, increasing the SINR threshold γ_{th} imposes more stringent decoding requirements, and therefore leads to a higher outage probability, as illustrated in Fig. 6. Likewise, smaller values of ζ, which correspond to more severe pointing errors, intensify beam misalignment and reduce the received optical power, thereby degrading the outage performance, as shown in Fig. 7. Across all considered scenarios, the strong user U_1 consistently achieves superior outage performance compared with the weaker user U_2, which is consistent with the expected behavior of NOMA systems under appropriate power-domain multiplexing and effective SIC operation.

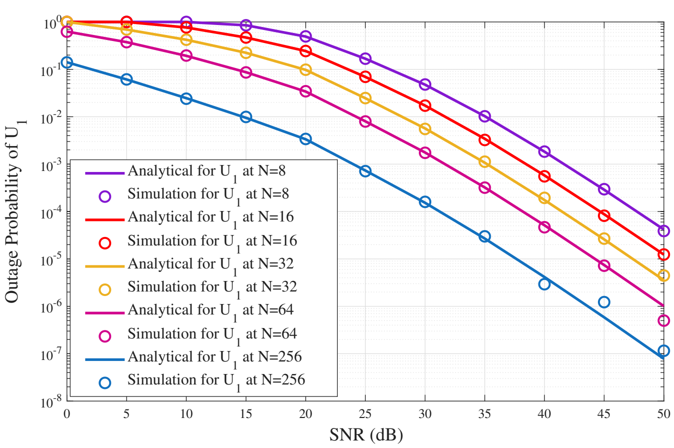

Fig. 5. Outage Probability of U_1 user at different N values.

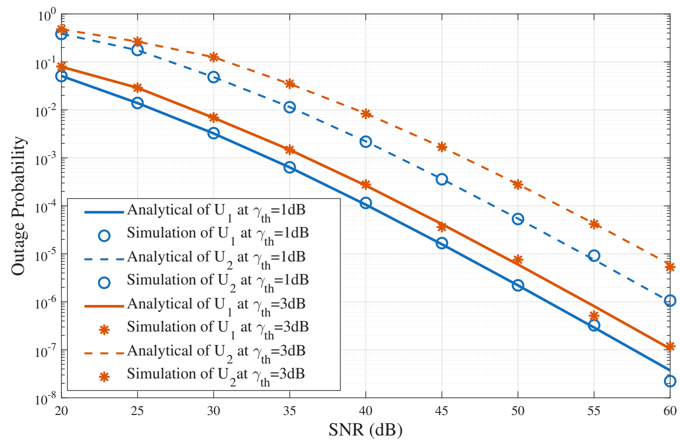

Fig. 6. Outage Probability of U_1 and U_2 users at different γ_{th} values.

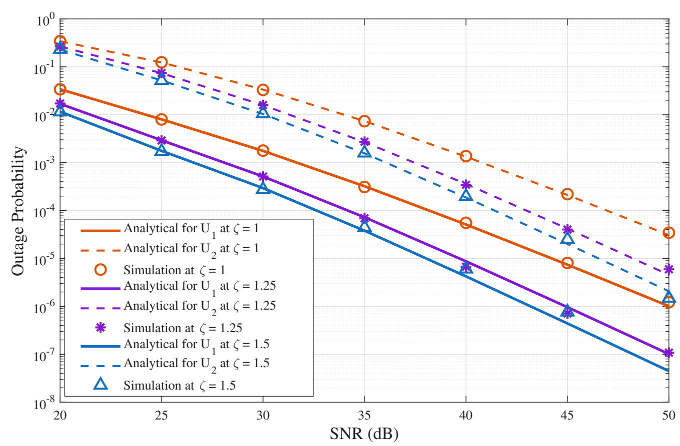

Fig. 7. Outage Probability of U_1 and U_2 users at different ζ values.

Figure 8 presents a comparative evaluation of the outage performance of U_1 with and without IRS, as well as that of U_2 with and without NOMA. This comparison is particularly useful for isolating the individual contributions of IRS and NOMA to the overall system performance. In accordance with

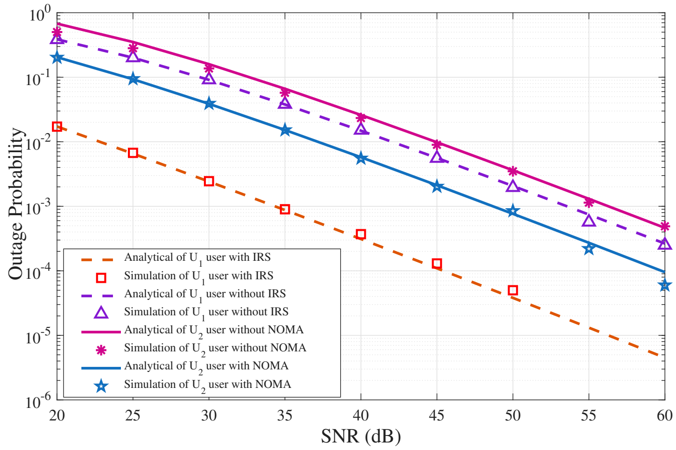

Fig. 8. Outage probability of U_1 user with and without IRS, and U_2 with and without NOMA.

theoretical expectations, the incorporation of IRS improves the effective channel quality of U_1 through intelligent signal reflection, thereby reducing the probability that the received SINR falls below the required decoding threshold. Similarly, the use of NOMA improves the outage performance of U_2 by enabling more efficient power-domain resource allocation and reception. Quantitatively, at an SNR of 30 dB, the outage probability of U_1 without IRS is approximately 0.1, whereas with IRS it decreases to nearly 0.001, corresponding to an improvement of two orders of magnitude. Likewise, for U_2, the outage probability decreases from approximately 0.45 in the absence of NOMA to about 0.045 when NOMA is employed. These observations clearly demonstrate that both IRS and NOMA make substantial and complementary contributions to performance enhancement, thereby confirming the effectiveness of their integration in improving the reliability of the proposed system.

Fig. 9 depicts the outage performance of U_1 as a function of the NLOS link distance for different values of the target SINR threshold γ_{th}. In accordance with theoretical expectations, the outage probability increases monotonically with distance, since the cumulative effects of attenuation, scattering, absorption, and geometric spreading progressively weaken the received optical signal over the extended NLOS path. It is also observed that lower values of γ_{th} yield improved reliability, as less stringent decoding requirements increase the probability of successful reception. Furthermore, beyond approximately 120 m, all outage curves exhibit a sharp rise, indicating the onset of a highly degraded transmission regime in which the combined channel impairments render reliable communication increasingly difficult. This behavior highlights the strong sensitivity of the NLOS-assisted link to propagation distance and underscores the importance of maintaining favorable channel conditions for sustained system reliability.

B. ABER vs SNR

Fig. 10 presents the ABER performance of both U_1 and U_2 under IRS-assisted and non-IRS transmission conditions. ABER is expected to decrease with increasing SNR because a stronger received signal improves the reliability of symbol detection and reduces the probability of decision error. This expected trend is clearly observed in the figure, where the ABER of both users decreases progressively as the SNR increases. In particular, at 20 dB, the ABER of U_1 in the proposed IRS-assisted system falls below 10^{-1}, whereas the corresponding non-IRS case remains at a significantly higher error level, close to 10^0. This marked difference indicates that the incorporation of IRS substantially improves the effective channel quality and mitigates the impact of fading and attenuation on detection accuracy. Therefore, the results in Fig. 10 confirm that IRS assistance provides a significant reduction in bit error rate and thereby enhances the overall transmission fidelity of the proposed system across the entire considered SNR range.

C. Impact of Water Turbidity

Fig. 11 illustrates the influence of bubble length (BL) on the outage probability of both users under saltwater and freshwater conditions. Based on the EGG parameter sets listed in Table IV, it is observed that the outage probability increases with BL, which is consistent with the theoretical expectation that stronger bubble activity intensifies scattering-induced turbulence and degrades the effective channel quality. At an SNR of 25 dB, the outage probability of U_1 in freshwater for BL $=$ 4.7 L/min is approximately 0.0045, whereas it increases to nearly 0.055 in saltwater for BL $=$ 16.5 L/min. For the same BL of 4.7 L/min, the outage probability of U_2 is considerably higher, at approximately 0.1, indicating the comparatively more vulnerable transmission condition of the far user. As the bubble length increases to 16.5 L/min, the outage probabilities of U_1 and U_2 further increase to approximately 0.055 and 0.45, respectively. These results clearly demonstrate that increasing BL has a detrimental effect on system reliability by aggravating underwater turbulence and weakening the received signal. Nevertheless, U_1 consistently achieves superior outage performance relative to U_2, which may be attributed to the IRS-assisted enhancement of the effective channel gain available to the near user.

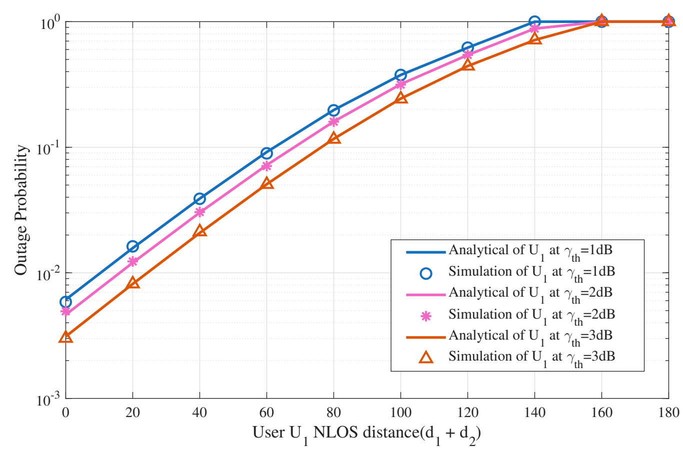

Fig. 9. Outage probability of U_1 with NLOS at a distance of $d = d_1 + d_2$.

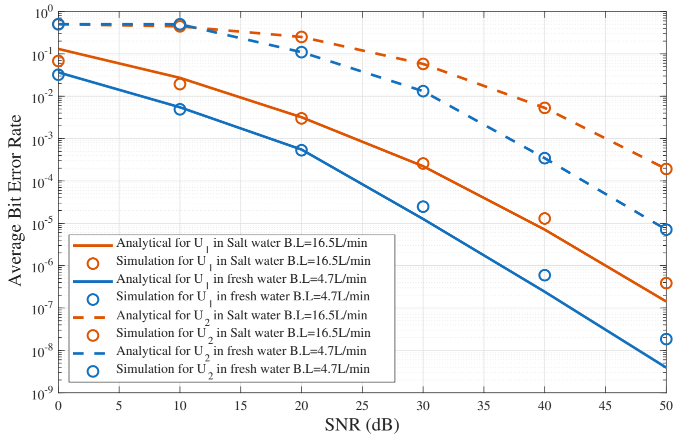

Fig. 10. Average bit error rate of the U_1 and U_2 users.

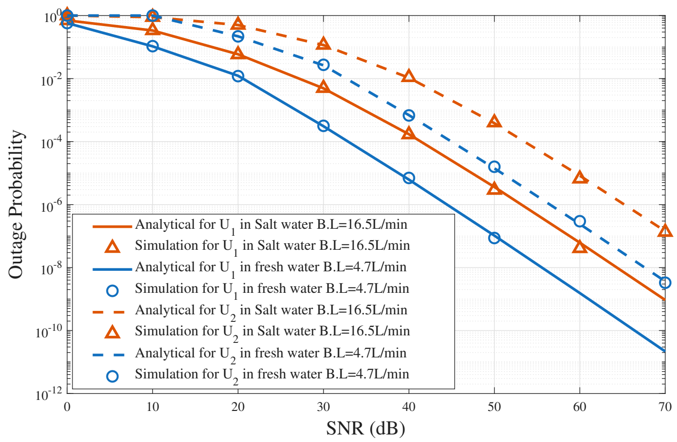

Fig. 11. Outage Probability of U_1 and U_2 users at different bubble lengths.

VI. Conclusion

In this paper, an IRS-assisted NOMA-based UVLC framework was investigated to enhance the reliability and efficiency of multi-user underwater optical communication under practical channel impairments. The proposed framework addresses the adverse effects of underwater turbulence, pointing errors, attenuation, and residual self-interference through the integration of IRS-aided signal reflection with NOMA transmission. Closed-form expressions for outage probability and ABER were derived using the EGG turbulence model and validated through Monte Carlo simulations. The results show that IRS deployment significantly improves the received signal quality and overall link reliability by reconfiguring the underwater optical propagation path. Specifically, increasing the number of IRS reflecting elements reduces outage probability and improves ABER performance, particularly in the high-SNR region. In contrast, severe bubble-induced turbulence degrades system performance, highlighting the sensitivity of UVLC links to underwater channel variations. Hence, the proposed IRS–NOMA-assisted UVLC framework offers an effective approach for improving spectral efficiency, link reliability, and user performance in future underwater optical wireless networks. Future work may focus on optimizing the IRS element size and adaptive resource-allocation strategies to maintain user fairness under varying underwater channel conditions.

Acknowledgments

The authors would like to thank the VIT-AP University for its institutional support throughout the development of this research.

References

[1] Z. Zeng, S. Fu, H. Zhang, Y. Dong, and J. Cheng, "A survey of underwater optical wireless communications," *IEEE Communications Surveys & Tutorials*, vol. 19, no. 1, pp. 204–238, 2017, doi: 10.1109/COMST.2016.2618841.

[2] V. L. Jayaweera, C. Peiris, D. Darshani, S. Edirisinghe, N. Dharmaweera, and U. Wijewardhana, "Visible light communication for underwater applications: Principles, challenges, and future prospects," *Photonics*, vol. 12, no. 6, 2025, doi: 10.3390/photonics12060593.

[3] A. S. Abrar and M. Rani, "Underwater visible light communication: recent advancements and channel modeling," *Journal of Optics*, pp. 1–15, 2025, doi: 10.1007/s12596-025-02839-9.

[4] J. Merin Joshiba, D. Judson, and V. Bhaskar, "A comprehensive review on noma assisted emerging techniques in 5g and beyond 5g wireless systems," *Wireless Personal Communications*, vol. 130, no. 4, pp. 2385–2405, 2023, doi: 10.1007/s11277-023-10384-6.

[5] L. Dai, B. Wang, Y. Yuan, S. Han, I. Chih-lin, and Z. Wang, "Non-orthogonal multiple access for 5g: solutions, challenges, opportunities, and future research trends," *IEEE Communications Magazine*, vol. 53, no. 9, pp. 74–81, 2015, doi: 10.1109/MCOM.2015.7263349.

[6] M. Jain, N. Sharma, A. Gupta, D. Rawal, and P. Garg, "Performance analysis of noma assisted underwater visible light communication system," *IEEE Wireless Communications Letters*, vol. 9, no. 8, pp. 1291–1294, 2020, doi: 10.1109/LWC.2020.2988887.

[7] M. Elamassie, L. Bariah, M. Uysal, S. Muhaidat, and P. C. Sofotasios, "Capacity analysis of noma-enabled underwater vlc networks," *IEEE Access*, vol. 9, pp. 153 305–153 315, 2021, doi: 10.1109/ACCESS.2021.3122399.

[8] K. W. S. Palitharathna, H. Suraweera, G. M. R. Godaliyadda, V. Herath, and J. Thompson, "Average rate analysis of cooperative noma aided underwater optical wireless systems," *IEEE Open Journal of the Communications Society*, vol. 2, pp. 2292 – 2310, 09 2021, doi: 10.1109/OJCOMS.2021.3116146.

[9] A. Kumar, S. Al-Kuwari, D. N. K. Jayakody, and R. Alkanhel, "Security performance analysis of a noma-assisted underwater vlc system under imprecise channel estimations," *IEEE Access*, vol. 10, pp. 117 021–117 032, 2022, doi: 10.1109/ACCESS.2022.3218049.

[10] Q. Wu, S. Zhang, B. Zheng, C. You, and R. Zhang, "Intelligent reflecting surface-aided wireless communications: A tutorial," *IEEE Transactions on Communications*, vol. 69, no. 5, pp. 3313–3351, 2021, doi: 10.1109/TCOMM.2021.3051897.

[11] K. Dolas and M. R. Bhatnagar, "On performance of irs-assisted hybrid satellite–terrestrial cooperative communication," *IEEE Transactions on Aerospace and Electronic Systems*, vol. 59, no. 2, pp. 2020–2028, 2023, doi: 10.1109/TAES.2022.3200930.

[12] Y. Ata, H. Abumarshoud, L. Bariah, S. Muhaidat, and M. A. Imran, "Intelligent reflecting surfaces for underwater visible light communications," *IEEE Photonics Journal*, vol. 15, no. 1, pp. 1–10, 2023, doi: 10.1109/JPHOT.2023.3235916.

[13] Y. Ata, X. Yi, Y. Li, X. Tao, and A. M. Vegni, "A unified channel model for irs-aided underwater owc with combined attenuation losses," *IEEE Journal on Selected Areas in Communications*, vol. 43, no. 5, pp. 1552–1567, 2025, doi: 10.1109/JSAC.2025.3543523.

[14] R. Salam, V. A. Bohara, and A. Srivastava, "Smart element allocation strategies for dynamic optical irs in underwater wireless communication," *IEEE Transactions on Vehicular Technology*, vol. 74, no. 3, pp. 4349–4361, 2025, doi: 10.1109/TVT.2024.3492284.

[15] A. Khan, S. A. H. Mohsan, A. Elfikky, A. I. Boghdady, S. Ahmad, and N. Innab, "A survey of intelligent reflecting surfaces: Performance analysis, extensions, potential challenges, and open research issues," *Vehicular Communications*, vol. 51, p. 100859, 2025, doi: 10.1016/j.vehcom.2024.100859.

[16] M. Jain, N. Sharma, A. Gupta, D. Rawal, and P. Garg, "Noma assisted underwater visible light communication system with full-duplex cooperative relaying," *Vehicular Communications*, vol. 31, p. 100359, 2021, doi: 10.1016/j.vehcom.2021.100359.

[17] M. F. Ali, D. N. K. Jayakody, S. Garg, G. Kaddoum, and M. S. Hossain, "Dual-hop mixed fso-vlc underwater wireless communication link," *IEEE Transactions on Network and Service Management*, vol. 19, no. 3, pp. 3105–3120, 2022, doi: 10.1109/TNSM.2022.3181169.
[18] A. Kumar and D. N. K. Jayakody, "Secure noma-assisted multi-led underwater visible light communication," *IEEE Transactions on Vehicular Technology*, vol. 71, no. 7, pp. 7769–7779, 2022, doi: 10.1109/TVT.2022.3167992.
[19] Q. Zhang, D.-W. Yue, and X.-Y. Xu, "Performance analysis of reconfigurable intelligent surface-assisted underwater wireless optical communication systems," *IEEE Photonics Journal*, vol. 16, no. 4, pp. 1–14, 2024, doi: 10.1109/JPHOT.2024.3407882.
[20] E. Zedini, H. M. Oubei, A. Kammoun, M. Hamdi, B. S. Ooi, and M.-S. Alouini, "Unified statistical channel model for turbulence-induced fading in underwater wireless optical communication systems," *IEEE Transactions on Communications*, vol. 67, no. 4, pp. 2893–2907, 2019, doi: 10.1109/TCOMM.2019.2891542.
[21] I. Gradshteyn and I. Ryzhik, *Table of Integrals, Series, and Products*, 7th ed. San Diego: Academic Press, 2007.
[22] Wolfram Research, *Meijer G-Function Properties*, Wolfram Functions Site, 2024, available at: http://functions.wolfram.com/07.34.02.0001.01.

Prathibha Praharsha Sripathi received the B.Tech. degree in Electronics and Communication Engineering and M.Tech. degree in Embedded Systems from JNTU Kakinada, India in 2013 and 2018 respectively. She is currently pursuing Ph.D. degree in School of Electronics Engineering at VIT-AP University, Amaravati, India. Her research interests include embedded systems, wireless communications, Underwater Visible Light Communications, NOMA, and IRS.

Mahesh Miriyala (Member, IEEE) received the B.Tech. degree in Electronics and Communication Engineering from JNTU Hyderabad, India, in 2009, the M.Tech. degree in Embedded Systems from JNTU Anantapur, in 2012, and the Ph.D. degree in Electronics and Communication Engineering from the National Institute of Technology Puducherry, Karaikal, India, in 2021.

He is currently working as an Assistant Professor in the School of Electronics Engineering at VIT-AP University, Amaravati, India.He is an IEEE member. His research interests include embedded systems, wireless communications, Internet of Things (IoT), IEEE 802.11ah, NOMA, and 5G networks. He has published several research articles in SCI/Scopus indexed journals and conferences and holds multiple patents in the areas of wireless communication and IoT. He has also contributed to book chapters and delivered technical talks and workshops on contemporary topics in communication and AI-enabled systems.